NASA TM X-52849

NASA TECHNICAL MEMORANDUM

NASA TM X-52849

COMPONENT TESTING OF A 30-CENTIMETER DIAMETER ELECTRON BOMBARDMENT THRUSTER

by Robert T. Bechtel
Lewis Research Center
Cleveland, Ohio

TECHNICAL PAPER proposed for presentation at
Eighth Electric Propulsion Conference sponsored by
American Institute of Aeronautics and Astronautics
Stanford, California, August 31 - September 2, 1970

COMPONENT TESTING OF A 30-CENTIMETER DIAMETER ELECTRON BOMBARDMENT THRUSTER

by Robert T. Bechtel

Lewis Research Center
Cleveland, Ohio

TECHNICAL PAPER proposed for presentation at

Eighth Electric Propulsion Conference
sponsored by the American Institute of Aeronautics and Astronautics
Stanford, California, August 31 - September 2, 1970

NATIONAL AERONAUTICS AND SPACE ADMINISTRATION

COMPONENT TESTING OF A 30-CENTIMETER DIAMETER ELECTRON BOMBARDMENT THRUSTER

Robert T. Bechtel
Lewis Research Center
National Aeronautics and Space Administration
Cleveland, Ohio

Abstract

A program to determine the effect of three critical components on Mercury electron-bombardment thruster performance is described. Various glass-coated accelerator grids, hollow cathode configurations, and plasma bridge neutralizer positions were tested with a 30-centimeter diameter mercury thruster. The grid with the smallest diameter accelerator hole was found to provide the maximum beam current, highest propellant utilization efficiency, and most stable operation. Cathodes with orifices about 0.8 mm diameter provided the best thruster performance consistent with long lifetime requirements. A neutralizer position pointing downstream at a 80° angle to the plane of the accelerator minimized the accelerator drain current.

Introduction

Electron-bombardment thrusters, which operate at input power levels of about 2 kilowatts and specific impulses of about 3000 seconds (net accelerating potential of 1000 volts), are currently of interest for future space flight applications.[1,2] The results of an initial optimization of a 30 centimeter diameter mercury thruster of this type have been detailed in references 3 and 4. The thruster typically operates at a discharge chamber loss of 200 electron volts per beam ion produced at a propellant utilization efficiency of greater than 90 percent. The use of a single, glass-coated accelerator grid permitted operation with this performance at specific impulses from 2000 to 3000 seconds.

More recent investigations have been extended to include detailed testing of individual thruster components. The results are reported in this paper. Three glass coated grid configurations were tested to determine their comparative performance and effect on thruster performance. Six cathodes were tested under similar thruster operating conditions to determine the effect of cathode diameter and orifice diameter on cathode lifetime. Four different cathodes were tested in a thruster equipped with a Langmuir probe to determine cathode effect on thruster performance. Finally the neutralizer was tested at different positions to determine its performance and effect on accelerator performance.

Apparatus and Procedure

The 30-centimeter diameter, electron-bombardment mercury thruster described in reference 3 was used for these tests. Fig. 1 is a sketch of this thruster. The thruster employs a SERT II type hollow cathode[5,6,7] and plasma bridge neutralizer.[6,7,8] The extraction system used was a 30-centimeter diameter glass-coated accelerator grid.[3,9] Sixteen permanent magnets were used to provide the magnetic field. The propellant vaporizer and feed system and the vacuum facility are detailed in reference 3.

The neutralizer tests and cathode lifetime tests were conducted in an 18.3 m long by 7.6 m diameter vacuum facility.[10] Cathode comparison and accelerator grid comparison tests were conducted in a 4.6 meter, 1.5 meter diameter vacuum facility.

For the glass coated grid evaluation tests, a stable thruster operating point was established first. This was followed by a variation in propellant flow rate or accelerating voltage. Critical parameters such as beam current and accelerator potential were monitored on an oscillograph to determine maxima or minima. All thruster operating voltages and currents were measured with 1 percent meters.

For the cathode evaluation tests, photographs were taken using a microscope with a magnification of 39 and 58. These photographs gave a comparison of the surface condition of the cathode tip and a measure of the orifice diameter at the tip surface before and after tests. Determining the minimum orifice diameter below the tip surface was not readily accomplished.

For the two 3.2 mm outside diameter cathodes, surface analyzer traces of the tip surface were made. The surface analyzer recorded the vertical motion of a stylus as it was run horizontally across the tip surface through the orifice diameter. Stylus depth movements as small as 2.5×10^{-5} mm were sensed by the electronics readout. This method provided good documentation of the tip surface before and after thruster testing. The beveling of the orifice very close to the surface can be measured with this technique, however, measurement of the orifice chamfer was limited to a depth of approximately 0.05 mm because of the width of the stylus.

A third method of orifice documentation suggested by Hughes Research Laboratories[4] involved the use of an elastic impression material which was forced into the orifice. The material is flexible enough after setting to generally be removed without deforming the impression.

Neutralizer data were obtained by varying the neutralizer propellant flow rate for a fixed neutralizer position and thruster operating point. Several neutralizer positions were tested with the same operating thruster.

A Langmuir probe was installed in an operating thruster to provide information on differences in thruster performance with various cathodes. The probe traces

TM X-52849

E-5780

were obtained with an electrically isolated microammeter and high impedance digital voltmeter system. The entire system was operated at a high common mode voltage, which produced some difficulties. Leakage currents of the order of a few microamps produced errors in the base level ion currents and slopes of the probe volt-ampere characteristics. These errors did not seriously effect the plasma potential values, obtained by graphical analysis and estimated to be accurate to ±0.5 volts.

Results and Discussion

Glass Coated Accelerator Grids

Important dimensional parameters of the grid configurations tested are shown in Table I. Each grid was tested at the same operating point to permit meaningful comparison of grid performance. During testing, a maximum beam current was found for each of the grids at a given operating voltage. Typical data are shown in Fig. 2. The maximum beam current for each grid is shown in Fig. 2(a). The beam current increased from 0.61A for the 3.6 mm diameter hole grid (grid A) to 1.97A for the 1.4 mm diameter hole grid (grid C). Extrapolation of the curve in Fig. 2(a) indicates that beam currents in excess of 2.4A may be possible by further reducing the coated grid hole diameter.

Fig. 2(b) shows the propellant utilization efficiencies at a beam current somewhat less than maximum. This was done to avoid the onset of the instability which defined the maximum beam current. The propellant utilization increased from 50 percent and approached 93 percent as the beam current increased from 0.42 to 1.5A.

Improvement realized by changing from grid A to grid B is associated with a decrease in both glass thickness and hole diameter. The l_c/d_c decreased from 0.50 to 0.44. Further improvement was realized by reducing the hole diameter without significantly changing the glass thickness (compare grid B and grid C). In this variation, the l_c/d_c increased from 0.44 to 0.81. There was an improvement in the maximum beam current and the propellant utilization when the hole diameter was decreased for both increasing and decreasing values of l_c/d_c. A grid with the same configuration as grid C was tested for 465 hours at a net accelerating potential of 1000 volts and beam current of 1.5A.

The effect of net accelerating potential on beam current is shown in Fig. 3. Grids A and B show a slight increase in beam current up to 1200 volts net accelerating potential and then a slight decrease as the voltage is increased to 1500 volts. Grid B was also tested at 2000 volts and stable operation was found at a beam current of 1.25 amperes. Grid C performance at 1000 volts is clearly superior to grids A and B.

The effect of discharge voltage and cathode emission current on performance of grid A is shown in Fig. 4. There is an increase in maximum beam current as the emission current was increased at constant discharge voltage and as the voltage increased at constant current. Fig. 4(a) shows that it might be possible to increase the beam by increasing the emission current beyond 10 amperes. But the high discharge losses and adverse effects on cathode lifetime make this approach undesirable. Fig. 4(b) shows that the maximum beam does not increase significantly above a discharge voltage of about 40 volts.

A major problem which was found to depend on grid geometry was electron backstreaming. Backstreaming involves a breakdown in the negative potential barrier at the accelerator which permits electrons from the hollow cathode-plasma bridge neutralizer or neutral beam plasma to flow to the discharge chamber which is at net accelerating potential. Backstreaming can occur as electron current through the grid apertures to the discharge chamber or around the neutralizer shield screen to the outer wall of the thruster body.

Each of the grids was tested for backstreaming at a beam current slightly less than the maximum. Fig. 5 shows the minimum negative potential required to provide an adequate backstreaming potential barrier as a function of the net accelerating potential. The broken lines are lines of constant R where R is the ratio of the net accelerating potential to the total potential difference between the discharge potential and accelerating potential, $R = V_I/(V_I + |V_A|)$.

Grid B operated without backstreaming at a slightly larger value of R than grid A (0.60 compared to ≈0.57). This result is somewhat inconclusive however since grid B was tested at only one net accelerating potential. There is a considerable reduction in accelerator potential required for grid C. However, grid C was run with a slightly modified neutralizer shield. This might have accounted for some of the improvement by preventing backstreaming around the neutralizer to the outer wall of the thruster body. The backstreaming limit for a 15-centimeter diameter glass coated grid of the same hole geometry[11] is also shown on Fig. 5 and agrees to within 75 volts with the results of grid C.

Under seemingly steady operating conditions periods of backstreaming lasting for several microseconds have been observed. An oscilloscope was used to investigate the performance of a grid similar to grid C for this condition. Backstreaming lasting for about 50μ sec was found to randomly occur from 0.5 to 30 times per second depending on neutralizer operation. High voltage probes were used to measure the net accelerating potential (V_I), accelerator potential (V_A), and neutralizer floating potential (V_G) relative to ground. Photographs of typical oscilloscope traces are presented in Fig. 6. All of the photographs were synchronized on the positive slope of the accelerator voltage (V_A becoming less negative). Fig. 6(a) shows the time relation between the three voltages measured. The accelerator voltage begins to decrease first. After about a two microsecond delay the accelerator voltage has reached a value of approximately -300 volts. This corresponds to the backstreaming limit of this type grid (Fig. 5). At this point, electron backstreaming begins and the net accelerating voltage and neutralizer floating potential begin to decrease (V_I becomes less positive, V_G becomes less negative). The cause of these voltage variations is the voltage drop across the series resistive impedance of

the power supplies as the currents vary.

Fig. 6(b) shows that the same time relationship exists for the currents as for the voltages. The accelerator drain current begins to increase at the same time as the accelerator potential begins to decrease in magnitude. After about one microsecond, the apparent beam current (which is equal to the neutralizer emission current) begins to increase in phase with the net accelerating potential decrease. The fact that the accelerator drain current increases while the neutralizer emission current (beam current) remains constant during the first microsecond indicates that the initial increase in the accelerator drain current is not due to ions from the neutralizer going to the negative accelerator. Thus the rise in accelerator drain current must be due to ion current directly from the discharge to the grid, or electron current from the grid to the discharge. Several possibilities exist which could account for this phenomenon. For example, extracted ions might be defocused and strike the downstream face of the accelerator grid, or voids in the glass might permit ions to strike the upstream face of the accelerator directly. A third possibility is electron current through the glass due to high volume conductivity or along the surface of the glass due to high surface conductivity.

The transients were also monitored for periods on the order of 100μ sec. It was found that the voltages and currents would reach the maximum variation in about 10μ sec. and return to normal operating conditions within 50μ sec. The accelerator potential varied from -500 to +150 volts. The net accelerating potential varied from 1000 to 400 volts. And, the neutralizer floating potential varied from -15 to +200 volts during the transient. The beam current (neutralizer emission current) and accelerator drain current reached maximum values of 9 and 3 amps respectively from nominal operating values of 1.5A and 33 mA.

These transients apparently are initiated by the accelerator drain current increase as described above. This in turn loads down the accelerator potential to less than the backstreaming limit, thus permitting the electron backstreaming to occur. The exact reason for the transient eventually clearing itself is not known. It is believed that the voltages which support the current transient are reduced to a value at which the current transient is extinguished. These voltages then increase to their original value and normal thruster operation is restored. The transients do not appear to adversely affect the "steady state" performance of the thruster although they may have a long range effect on durability. A method for eliminating the transients remains to be developed.

The glass coated grid investigations have shown that the smallest diameter coated holes tested provided the highest beam current and propellant utilization efficiency obtained. In addition, the accelerator potential required to prevent electron backstreaming was lowest for the smallest diameter holes. Transient arcs, lasting for approximately 50μ sec were found to occur. High accelerator drain currents and electron backstreaming currents accompanied these arcs. The cause of the arcs and their long range effect on performance has not been determined.

Cathode Configurations

Cathode Lifetime. Two 3.2 mm outside diameter and four 6.3 mm outside diameter cathodes were tested. Initial orifice diameters ranged from 0.27 to 0.89 mm (10.6 to 35.0 mils). The cathodes tested are listed in Table II along with the critical dimensions at various times of operation. Fig. 7(a) shows the profile of the cathode orifices determined from the molds taken at the end of each cathode test. Fig. 7(b) shows a surface analyzer traces of the tip surface near the orifice for cathodes 5 and 6. The cathodes were operated at emission currents from 7.5 to 10.0A and discharge voltages from 35 to 42 volts.

Fig. 8 shows the variation in minor and major orifice diameter with time for 6.3 mm outside diameter cathodes. The plot of minor diameter (Fig. 8(a)) shows that the orifice actually closes with time for the smallest orifice (cathode 1). The minor diameter tends to increase with time for cathodes having a larger initial orifice diameter. The rate of increase for the two 0.8 mm orifice cathodes (3 and 4) is approximately 0.0003 to 0.0007 mm/hr. The plot of major diameter versus time (Fig. 8(b)) shows that for the smaller orifice cathodes (1 and 2), the major diameter increases at a high rate. For cathodes 3 and 4, the major orifice diameter increases at a much smaller rate (see Table II). Thus, for the smallest initial orifice diameter tested, the minor diameter decreased and the major diameter increased with run time. As the initial orifice diameter was made larger, the minor diameter rate of decrease became less and the major diameter rate of increase became less. For the largest initial orifice diameter tested both the minor and major orifice diameters increased at nominally the same rate.

The orifice diameter for the two 3.2 mm outside diameter cathodes (5 and 6) as a function of time is shown in Fig. 9. As for the case of the 6.3 mm outside diameter cathodes, the larger orifice diameter cathode (6) exhibits less of an orifice change with time. Cathode 5 (0.34 mm diameter orifice) was run for a total of 201 hours. A large increase in orifice diameter occurred within the first 10 hours. The major orifice diameter continued to increase beyond this time but at a rate which was more than an order of magnitude less than the initial rate. The minor diameter was decreasing during this test, although accurate measurements were not obtained.

The rate of increase of the major orifice diameters are shown in Fig. 10 as a function of initial orifice diameter. These rates were determined from the results of Figs. 8 and 9 for cathodes 1 thru 5. Cathode 6 showed a slight decrease in orifice diameter during the 15 hour test. An average rate of increase for cathode 5 is shown for the first 8.4 hours of test and for the full 201 hours of test, and illustrates the order of magnitude reduction in the rate of increase over a longer test time. For the 6.3 mm outside diameter cathodes, the rate of increase decreases an order of

magnitude for every 0.2 mm of initial orifice diameter increase.

Although cathode wear rates are undoubtedly related to thruster operating conditions, some general conclusions can be drawn from the data of Figs. 7 to 10. Cathodes having larger initial orifice diameters wear at slower and more uniform rates. Small orifice cathodes have a tendency to close near the upstream end of the tip while opening up near the downstream end. Small orifice cathodes wear very rapidly during the initial hours of test but the wear rate decreases by an order of magnitude after a couple of hundred hours of operation. Surface analyzer traces of a 3.2-millimeter diameter cathode indicate a chamfering of the surface around the orifice for both large and small orifices.

From these cathode tests it appears that an orifice of ~0.8 millimeter diameter provides the best possibility for extended lifetime for the following reasons. No change in the tip thickness was noted. The orifice wore at about the same rate at all depths. No closing of the orifice was noted. At the observed wear rate of 3×10^{-4} mm per hour calculations show that a 40 percent enlargement (0.3 mm) of the orifice would occur in 10^3 hours. This would result in a 1.1 millimeter major diameter orifice. If it is assumed that there is an order of magnitude reduction with time in the rate of increase similar to that experienced by cathode 5 (Figs. 9 and 10), the resulting orifice diameter would approach 1.3 mm after 10^4 hours, making this cathode design an acceptable geometry. King and Poeschel[4] have observed that initial chamfering of the cathode orifice resulted in a wear rate of the major orifice diameter of 4×10^{-5} mm/hr. Thus chamfering of the upstream cathode face may be a way to eliminate the large orifice rate of increase experienced in the first several hundred hours of operation with some cathodes.

Thruster Performance

During the investigation of cathode lifetime, it was noted that thruster performance differed from one cathode configuration test to another for the same discharge chamber configuration. It was found that different cathodes provided different discharge losses for the same main propellant flow, emission current, and propellant utilization efficiency. The larger orifice cathodes generally required less total power to produce the same beam current under the same nominal operating conditions.

To further investigate these performance differences a Langmuir probe was installed inside the distributor pole piece. The probe dimensions and location are given in Fig. 11. Four cathodes were tested with the Langmuir probe and are detailed in Table III. Each cathode was tested in the same thruster configuration at the same main propellant flow and emission current. The cathode propellant flow rate was varied from 0.035 A to 0.51 A equivalent mercury flow and Langmuir probe potential with respect to the cathode, the probe current, the beam current, and the discharge voltage were recorded. The data are shown in Fig. 12. The discharge chamber losses (Fig. 12(a)), plasma potential inside the distributor pole piece (Fig. 12(b)), and discharge voltage (Fig. 12 (c)) all exhibited a general decrease as the cathode orifice initial diameter increased. The effect of cathode outside diameter on thruster performance can be seen by comparing cathodes 7 and 8. The cathode orifice diameters differ by only 0.05 mm. The 3.2 mm outside diameter cathode shows slightly better performance than the 6.3 mm cathode, especially at propellant utilizations below approximately 90 percent where there is also a difference in the shape of the curves.

It is believed that the plasma potential inside the distributor pole piece is a measure of the voltage drop required to extract a given amount of emission current, in this case 8.0 A. As the cathode orifice diameter is increased this voltage requirement is reduced as illustrated in Fig. 12(b). This, in turn, reduces the fraction of the total discharge power expended in the region of the cathode. From Fig. 12(b), this power loss ranged from 176 watts (cathode 1, 22 volts and 8 amperes) to 86 watts (cathode 9, 10.8 volts and 8 amperes).

A further indication that the orifice size affects the emission characteristics is shown in Fig. 12(d). The cathode keeper configuration (Fig. 1) was the same for each test. A current of 0.5 A was drawn to the keeper electrode in each test. The voltage required to draw this current decreased as the initial orifice diameter was increased. Comparison of Figs. 12(b) and 12(d) shows that the plasma potential and keeper voltage vary by approximately the same amount with cathode changes.

Comparison of thruster performance with each of the cathodes tested was made after correcting for the power loss in the distributor pole piece region. This was done by subtracting the plasma potential from the discharge chamber voltage, and using this modified discharge voltage to determine a modified discharge chamber loss. These modified values are shown in Fig. 13 as a function of the propellant utilization efficiency. Data for the same diameter cathode tend to determine unique curves which have minimums about the same values. It is felt that the modified discharge chamber voltage (Fig. 13(b)) is a more representative measure of the potential difference across the baffle region (Fig. 11) than the total discharge chamber voltage. Furthermore, if the electrons become sufficiently randomized within the distributor pole piece such that the electron temperatures are on the order 2 eV[12], then the modified discharge chamber voltage is also a better measure of the primary electron energy in the main discharge. This would explain the similarity of thruster performance based on the modified discharge chamber voltage and the dissimilarity based on the total discharge chamber voltage (for example, compare Figs. 12(c) and 13(b)).

Conclusions drawn from Langmuir probe data in complex discharges such as reported here are subject to limitations. For example, the data gives values of plasma potential at only a single point whereas measurements throughout the chamber have shown voltage gradients on the order of 10 percent of anode potential to exist.[12,13] In addition, although cathodes were operated at the same cathode power, they were not necessarily at the same temperature because the thermal conduction

losses vary with configuration. It is possible that the cathode temperature may effect the emission characteristics.[14] The probe data do strongly suggest, however, that there is a significant voltage drop across the cathode - cathode keeper sheath needed to extract the desired emission current. The associated energy loss may be on the order of 50 percent of the total discharge energy required to produce the ion beam. Both the improvement in performance and the effect of the orifice diameter on cathode lifetime indicate an orifice of at least 0.8 millimeter diameter, or possibly larger, provides best overall thruster performance.

Neutralizer Performance

During one glass coated grid test, various neutralizer positions were tested to determine the effect on accelerator and neutralizer performance. The neutralizer was a SERT II type.[6,7,8] The cathodes were 3.2-millimeter outside diameter with a nominal orifice diameter of 0.28 millimeters. The neutralizer positions tested are given in Table IV. The position is defined by the tip axial distance from the accelerator, radial distance from the last row of accelerator holes, and angle of the neutralizer with the plane of the accelerator. The thruster was operated at a net accelerating potential of 1000 volts, beam current of 1.5 amperes, and accelerator voltage of -500 volts. The neutralizer keeper current was maintained at 0.8 amperes for stability, but was tested to as low as 0.2 ampere with no variation in neutralizer operating voltage.

The effect of neutralizer position is shown in Fig. 14. The neutralizer keeper voltage and floating potential vary strongly with neutralizer flow rate for both positions having a 24° angle (positions 1 and 2). Moving the neutralizer away from the beam axis from position 1 to 2, caused an increase in these voltages at all flow rates investigated. Subsequent increases in the neutralizer angle at the 2.5 by 2.5 cm position (2 thru 4) caused a general reduction in these voltages. Over the range of flow rates tested, the voltages were constant to within a volt for both the 50° and 80° cases (3 and 4), with the 80° case providing the best performance.

The influence of neutralizer position and flow rate on the frequency of the transient arcs (Fig. 6) is shown in Fig. 15. These arcs were measured with an event-per-unit-time meter. They were found to be random, but an average over 100 sec. seemed to give a representative arcing rate. Moving the neutralizer from position 1 to 2 caused an order of magnitude increase in the arcing rate. However, the subsequent increase in neutralizer angle reduced this arcing rate to about 1/sec.

The effect of neutralizer angle on accelerator drain current is shown in Fig. 16. A significant portion of the drain current is believed to be due to charge exchange ions formed in the region of the neutralizer. This is especially true for high neutralizer flow rates.[6] To some extent the base level drain current was dependent on the test run time which varied from test to test. More important in Fig. 16 is the trend of the data. Positions 1 and 2 (24° angle) exhibit an increase in drain current as the flow rate is increased. Position 3 (50° angle) actually shows a decrease in drain current with increased flow rate. This may be due to the change in the thermal condition of the grid during the time the data was taken. Further increasing the angle to 80° (position 4) resulted in a constant drain current over the range of flow rates tested. In general, the drain current tended to decrease as the neutralizer angle was increased. It may be that the differences in the shape of both the operating voltage curves (Fig. 14) and drain current curves (Fig. 16) for the 24°, 50°, and 80° positions are due to a reduced interaction between accelerator and neutralizer as the angle was increased. The general conclusion is that an increase in angle which points the tip further downstream from the accelerator significantly reduces the charge exchange impingement current and reduces the neutralizer operating voltages.

Conclusion

Tests were conducted with three major components of a 30 centimeter diameter thruster. Three glass-coated accelerator grids were tested. Electron backstreaming limits, both of a transient (50μ sec) and steady state nature, and maximum beam current which could be extracted were determined. Highest beam currents and propellant utilization efficiencies were obtained with the grid having the smallest diameter holes.

Cathode orifice diameter was found to affect both thruster performance and cathode wear. Larger orifices were found to wear at a slower rate when operated in the emission current range of interest, 7.5 to 10 amperes. Larger orifices were also found to lower the plasma potential within the distributor pole piece, and correspondingly reduce the discharge chamber losses. Cathodes having orifice diameters ~0.8 millimeter appear to provide good performance, consistent with long life. Smaller outside diameter cathodes resulted in somewhat better thruster performance, but durability remains to be evaluated.

Various neutralizer positions were tested to determine the effect on neutralizer operating voltages and accelerator charge-exchange drain current. A neutralizer angle of 80° to the accelerator plane resulted in the lowest valves accelerator drain current, neutralizer keeper voltage and floating potential

References

1. Barber, T. A., Goldsmith, J. V., and Edberg, J. R., "Spacecraft Flectric Propulsion - Now?," Astronautics and Aeronautics, Vol. 6, No. 6, June 1968, pp. 38-47.

2. Reader, P. D. and Regetz, J. D., Jr., "A Delta Boosted, Electrically Raised High Power Synchronous Satellite," Paper 69-1104, Oct. 1969, AIAA, New York, N. Y.

3. Bechtel, R. T., "Performance and Control of a 30-Cm-Diam, Low-Impulse, Kaufman Thruster," Journal of Spacecraft and Rockets, Vol. 7, No. 1, Jan. 1970, pp. 21-25.

4. King, H. J. and Poeschel, R. L., "Low Specific Impulse Ion Engine," NASA-CR-72677, Feb. 1970, Hughes Research Labs., Malibu, Calif.

5. Bechtel, R. T., Csiky, G. A., and Byers, D. C., "Performance of a 15-Centimeter Diameter, Hollow-Cathode Kaufman Thrustor," Paper 68-88, Jan. 1968, AIAA, New York, N. Y.

6. Byers, D. C. and Staggs, J. F., "SERT II-Thruster System Ground Testing," Journal of Spacecraft and Rockets, Vol. 7, No. 1, Jan. 1970, pp. 7-14.

7. Kerslake, W. R., Byers, D. C., and Staggs, J. F., "SERT II-Mission and Experiments," Journal of Spacecraft and Rockets, Vol. 7, No. 1, Jan. 1970, pp. 4-6.

8. Rawlin, V. K. and Pawlik, E. V., "A Mercury Plasma-Bridge Neutralizer," Journal of Spacecraft and Rockets, Vol. 5, No. 7, July 1968, pp. 814-820.

9. Banks, B., "Composite Ion Accelerators Grids," presented at the Electrochemical Society Third International Conference on Electron and Ion Beam Science and Technology, Boston, Mass., May 6-9, 1968.

10. Finke, R. C., Holmes, A. D., and Keller, T. A., "Space Environment Facility for Electric Propulsion Systems Research," TN D-2774, 1965, NASA, Cleveland, Ohio.

11. Banks, B. A. and Bechtel, R. T., "1000 Hour Endurance Test of a Glass Coated Accelerator Grid on a 15-Centimeter Diameter Kaufman Thruster," NASA TN D-5891, 1970.

12. Knauer, W., Poeschel, R. L., King, H. J., and Ward, J. W., "Discharge Chamber Studies for Mercury Bombardment Ion Thrusters," NASA-CR-72440, Sept. 1968, Hughes Research Labs., Malibu, Calif.

13. Masek, T. D., "Plasma Properties and Performance of Mercury Ion Thrusters," Paper 69-256, Mar. 1969, AIAA, New York, N. Y.

14. Rawlin, V. K. and Kerslake, W. R., "SERT II-Durability of the Hollow Cathode and Future Applications of Hollow Cathodes," Journal of Spacecraft and Rockets, Vol. 7, No. 1, Jan. 1970, pp. 14-20.

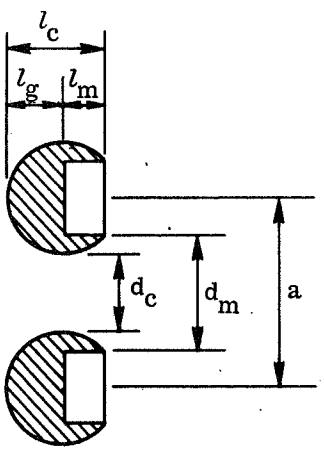

Grid	a, mm	d_c, mm	d_m, mm	l_c, mm	l_m, mm	l_g, mm	$\frac{l_c}{d_c}$	Percent open area of grid	
								Uncoated	Coated
A	5.63	3.55	4.00	1.78	0.76	1.01	0.50	45.9	36.1
B	4.25	2.75	3.18	1.19	.38	.81	.44	50.2	37.5
C	2.54	1.42	1.90	1.13	.38	.76	.81	51.0	28.4

TABLE I. - SUMMARY OF GLASS COATED GRID CONFIGURATIONS TESTED

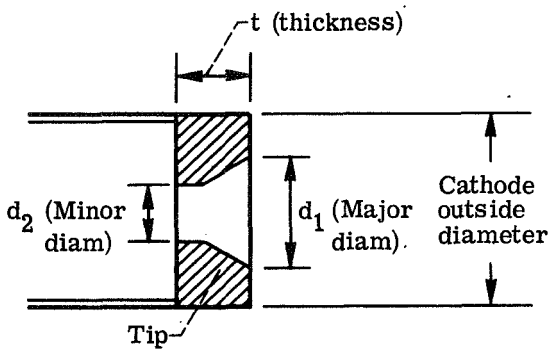

Cathode number	Cathode outside diameter, mm	Hours of test	Orifice diameter, mm				Tip thickness, t, mm		Major diameter rate of increase, mm/hr
			d_1 (major)		d_2 (minor)				
			(a)	(b)	(a)	(b)	(b)	(c)	
1	6.3	0	0.27	---------	0.27	----	----	1.27	------
		7.8	1.43	---------	.21	----	----	----	------
		9.5	1.28	1.44/1.18	.17	----	0.53	1.27	0.126
2	6.3	0	0.39	---------	0.39	----	----	1.27	------
		39.0	1.53	1.56/1.35	~0.35	0.43	1.28	1.22	0.029
3	6.3	0	0.79	---------	0.79	----	----	1.27	------
		50.1	.80	---------	.80	----	----	----	------
		69.5	.83	---------	.83	----	----	----	------
		89.7	.81	---------	.81	----	----	----	------
		132.6	.81	1.10/0.82	.81	0.80	----	1.24	0.0002
4	6.3	0	0.83	0.78	0.83	0.75	1.07	1.27	------
		144.0	.88	0.88/0.82	.88	.85	1.35	1.20	0.0003
5	3.2	0	0.34	---------	0.34	----	----	----	------
		8.4	.96	---------	.44	----	----	----	------
		108.1	1.32	---------	.57	----	----	----	------
		201.1	1.75	2.49/1.70	.31	0.41	1.15	1.06	0.007
6	3.2	0	0.89	---------	0.89	----	----	----	------
		15.6	.88	1.00/0.87	.88	0.82	1.12	1.15	------

[a]Determined by photomicrograph.
[b]Determined by orifice mold.
[c]Micrometer measurement.

TABLE II. - SUMMARY OF CATHODES TESTED

Cathode number	Cathode outside diameter, mm	Tip thickness, mm	Orifice diameter, mm	
			d_1 (major)	d_2 (minor)
[a]1	6.3	1.27	1.28	0.17
7	6.3	1.27	.84	.78
8	3.2	1.03	.89	.83
9	3.2	1.27	1.43	1.27

[a]Dimensions after ~9.5 hr testing (table I).

TABLE III. - SUMMARY OF CATHODES TESTED WITH LANGMUIR PROBE THRUSTER

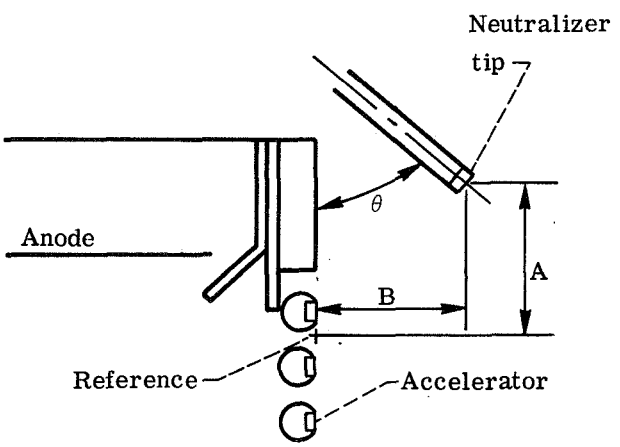

Position	A, cm	B, cm	θ, deg
1	0	3.8	24
2	2.5	2.5	24
3	2.5	2.5	50
4	2.5	2.5	80

TABLE IV. - SUMMARY OF NEUTRALIZER POSITIONS TESTED

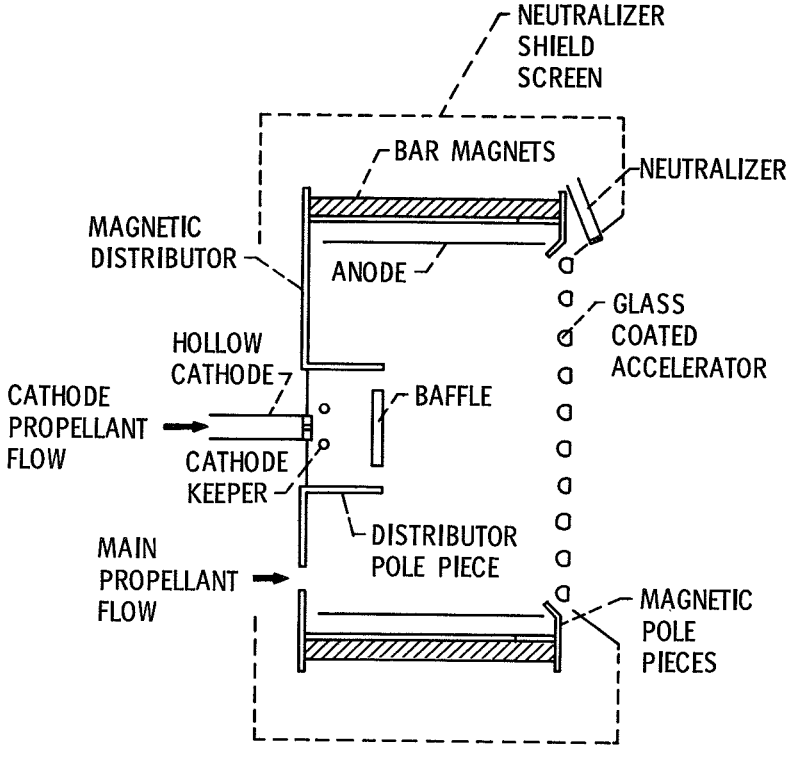

Figure 1. - Sketch of 30-centimeter diameter electron bombardment thruster.

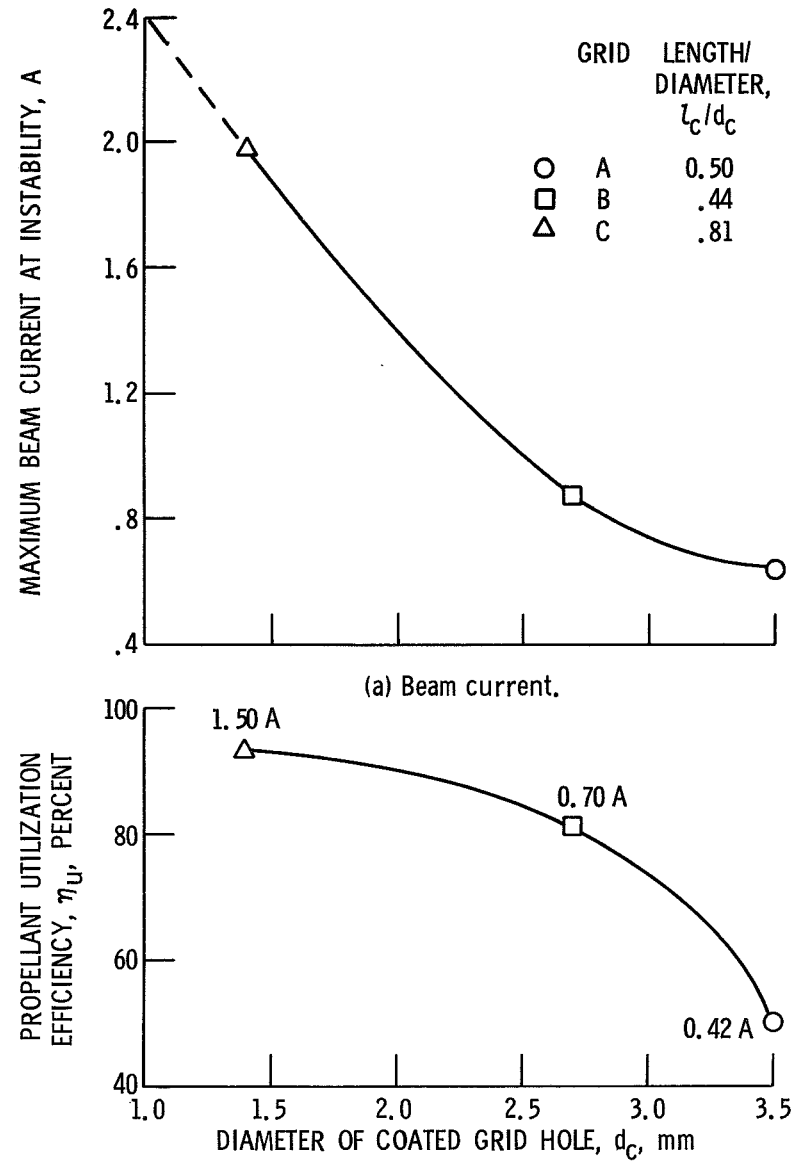

(a) Beam current.

(b) Propellant utilization efficiency.

Figure 2. - Effect of grid hole size on beam current and propellant utilization efficiency. Net accelerating potential, 1000 V; accelerator potential, 1000 V; emission current, 10 A; discharge voltage, 40 V.

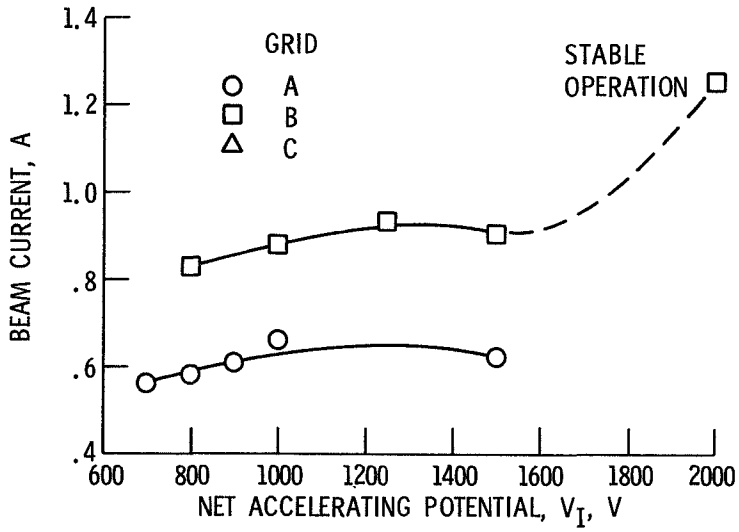

Figure 3. - Effect of net accelerating potential on beam current. Accelerator potential, 1000 V; emission current, 10 A; discharge voltage, 40 V.

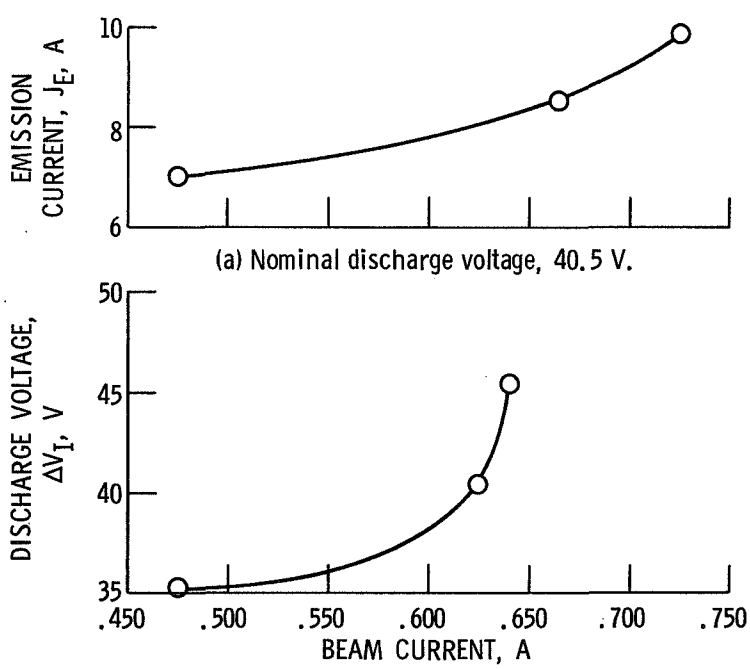

Figure 4. - Effect of discharge chamber operation on beam current for grid A. Net accelerating potential, 1000 V.

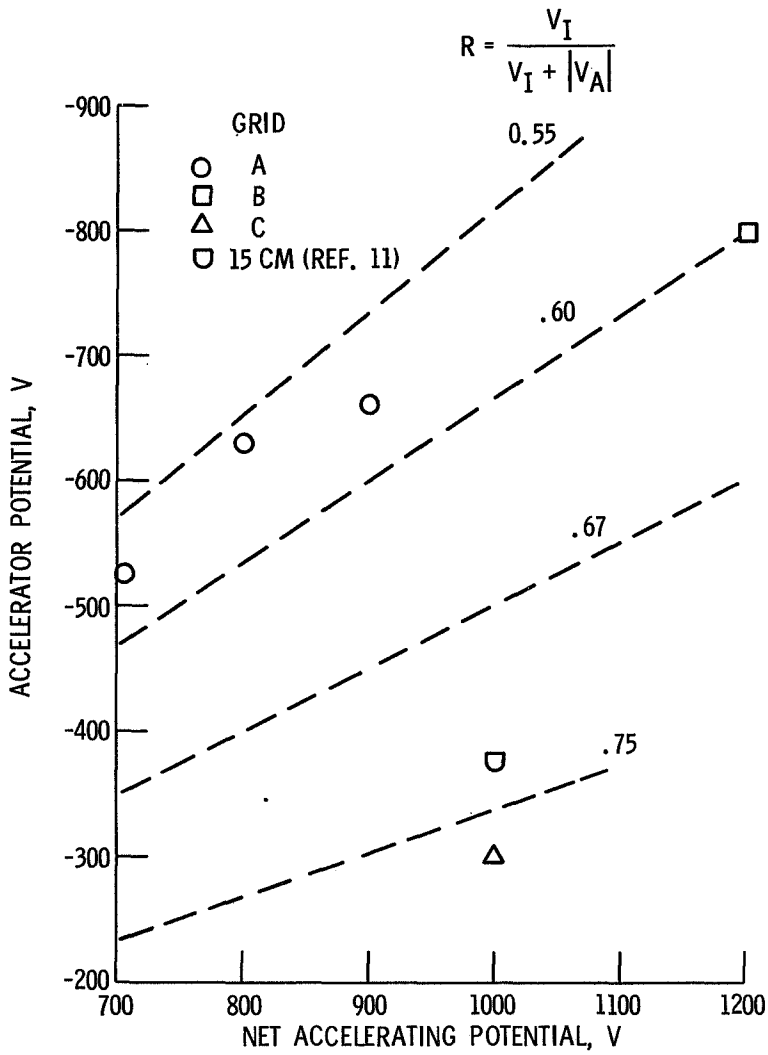

Figure 5. - Accelerator potential required to prevent electron backstreaming for various net accelerating potential.

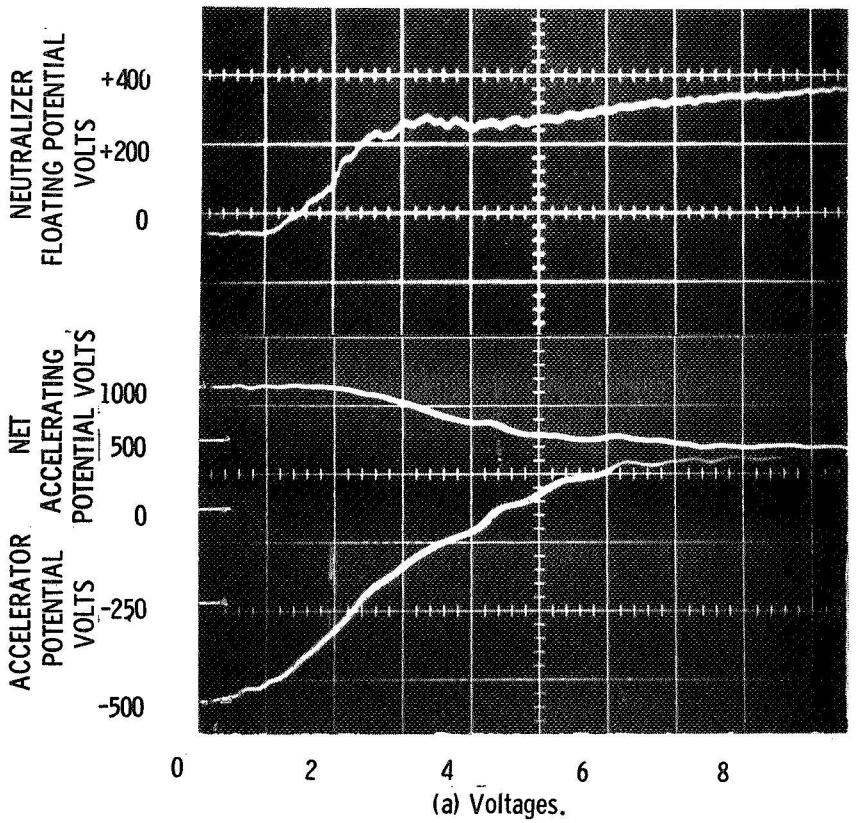

(a) Voltages.

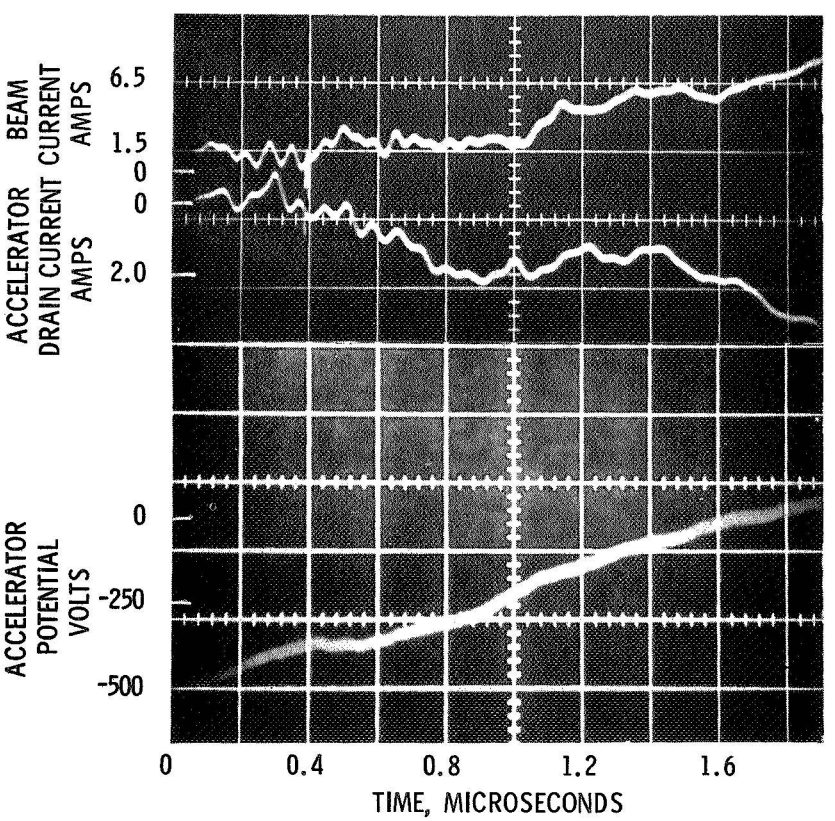

(b) Currents.

Figure 6. - Oscilloscope traces showing time variation of grid parameters during transient arc. Traces synchronized on positive slope of accelerator potential.

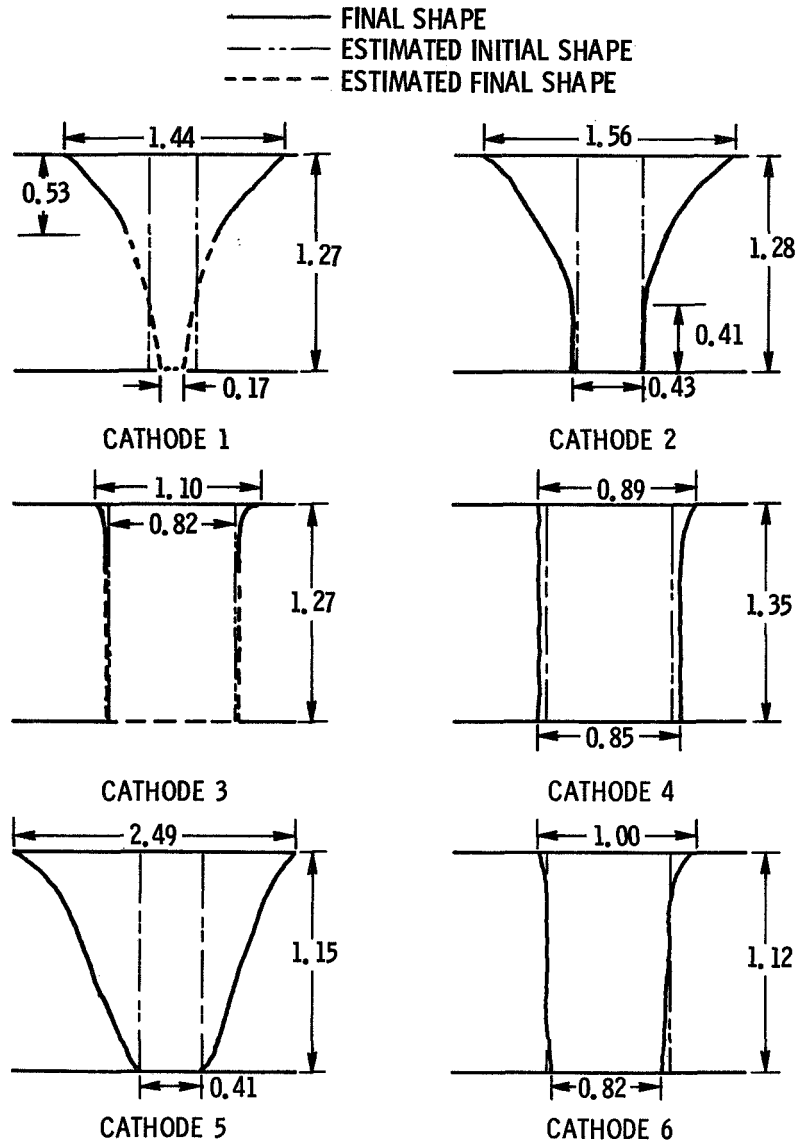

(a) Orifice contours from impressions.

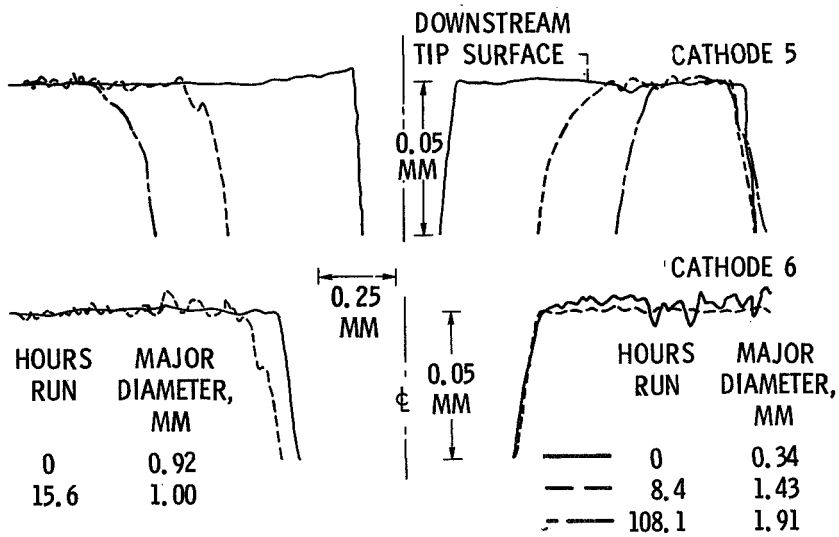

(b) Surface analyzer traces of the 3.2 mm outside diameter cathodes (note different vertical-horizontal scales).

Figure 7. - Profiles of cathodes. All dimensions in millimeters.

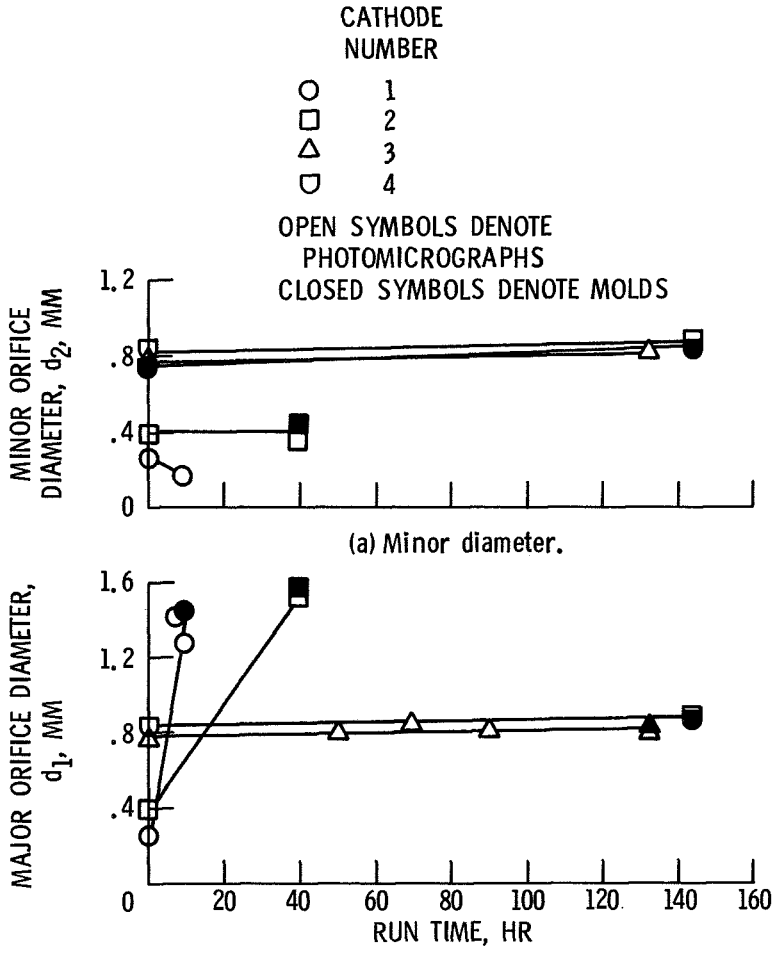

Figure 8. - Diameter of cathode orifice as function of time for 6.3 mm outside diameter cathodes (see table III).

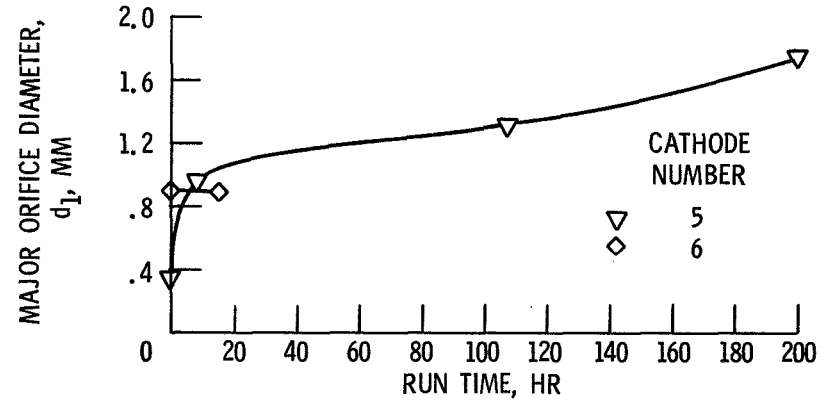

Figure 9. - Cathode orifice diameter for 3.2 mm diameter cathodes as a function of time.

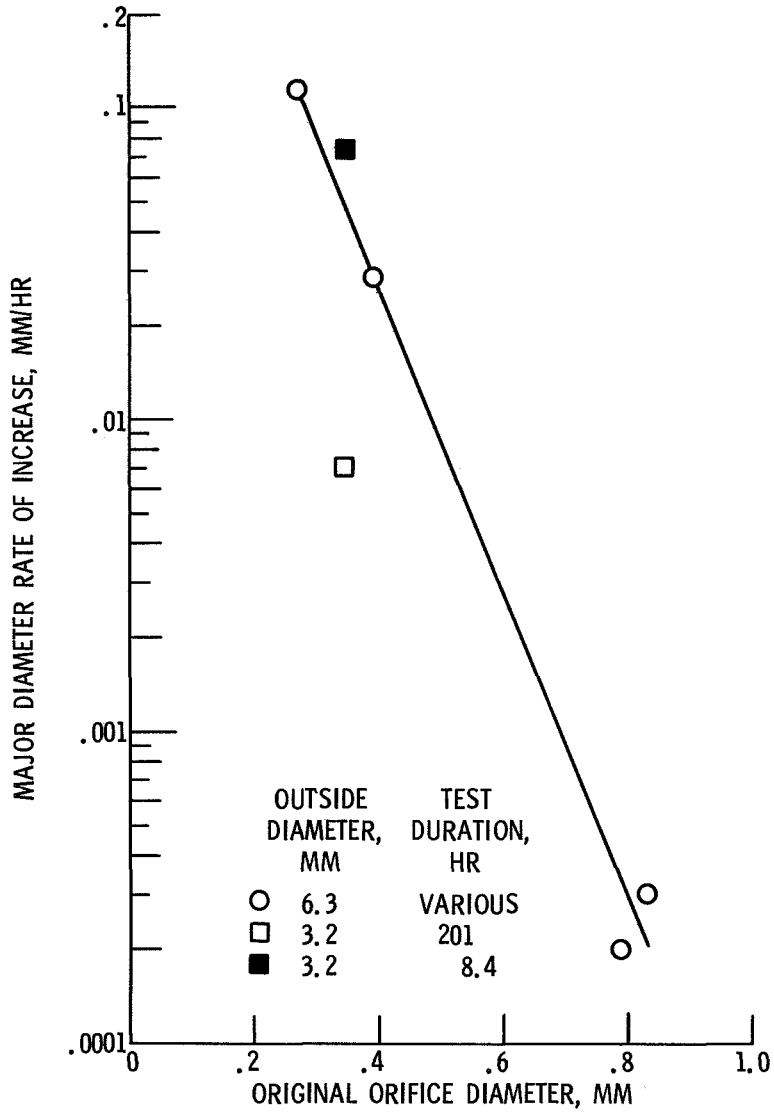

Figure 10. - Wear rate of cathode orifice major diameter as function of initial diameter.

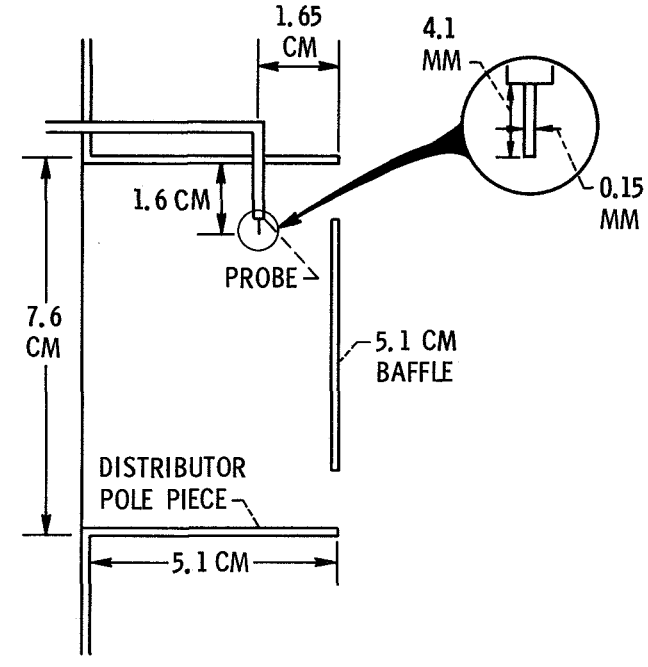

Figure 11. - Langmuir probe configuration.

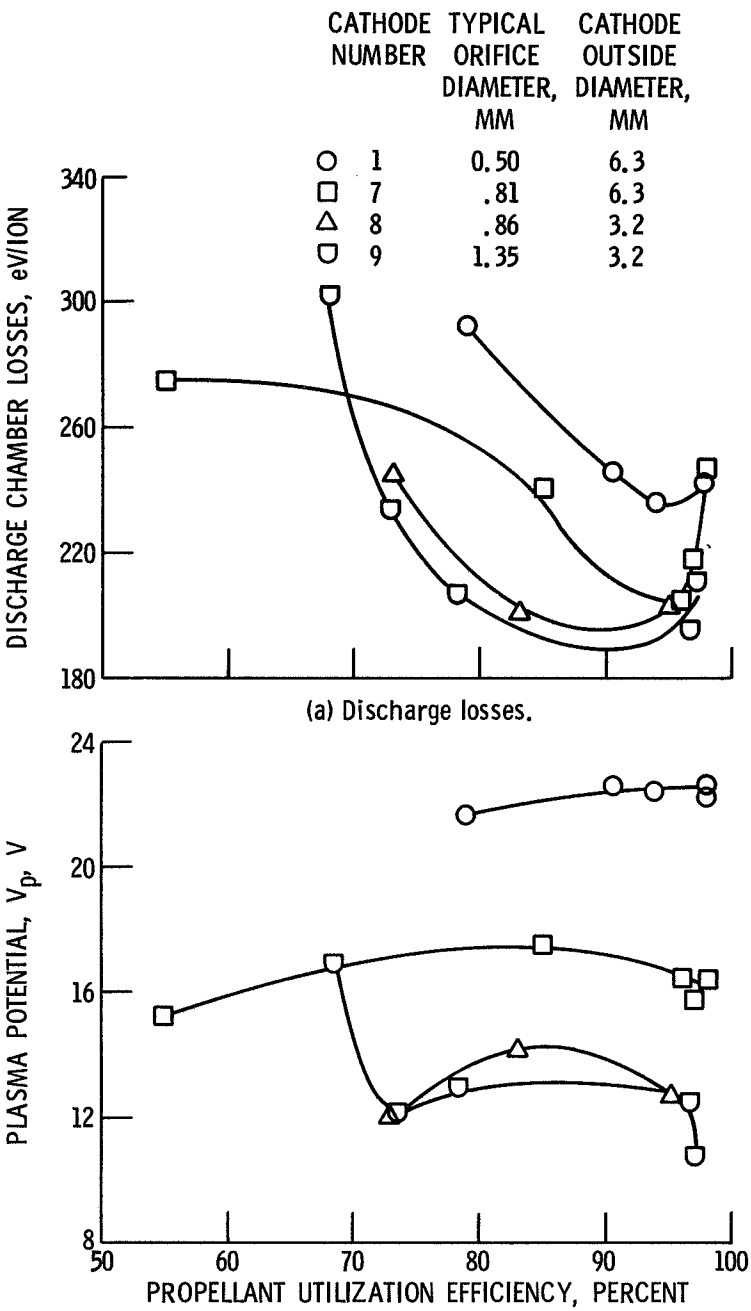

(a) Discharge losses.

(b) Plasma potential.

Figure 12. - Thruster operating parameters for different cathodes as a function of propellant utilization efficiency; emission current, 8 A.

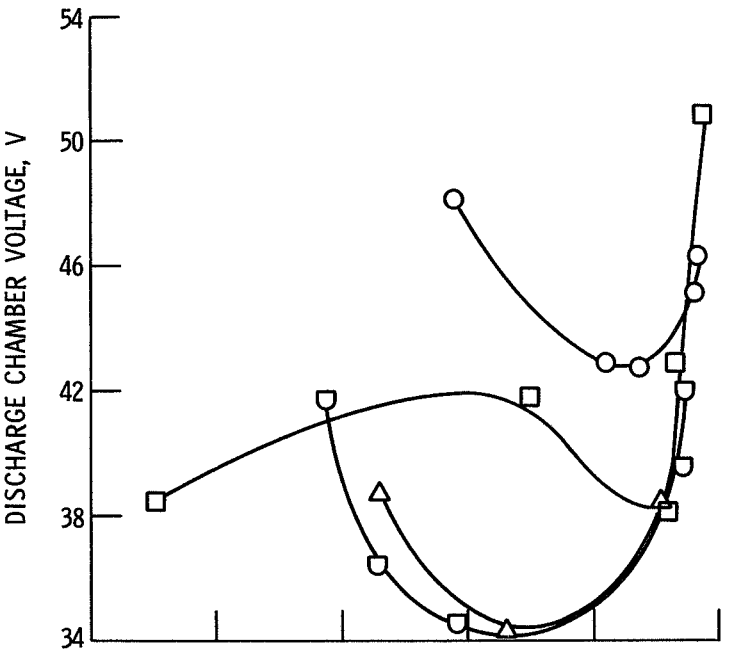

(c) Discharge voltage.

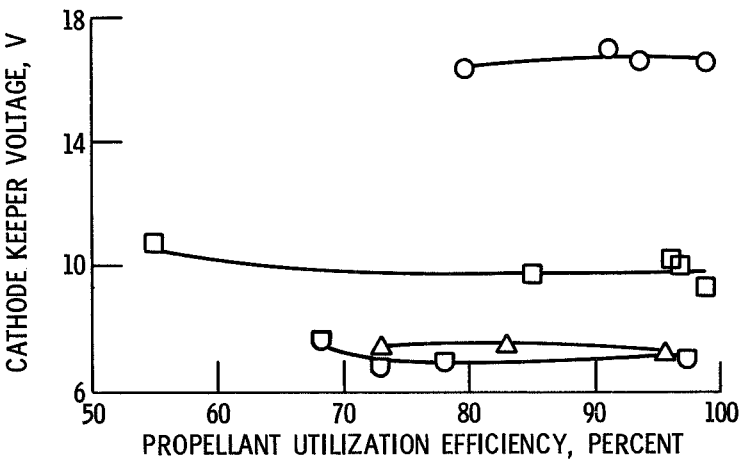

(d) Keeper voltage.

Figure 12. - Concluded.

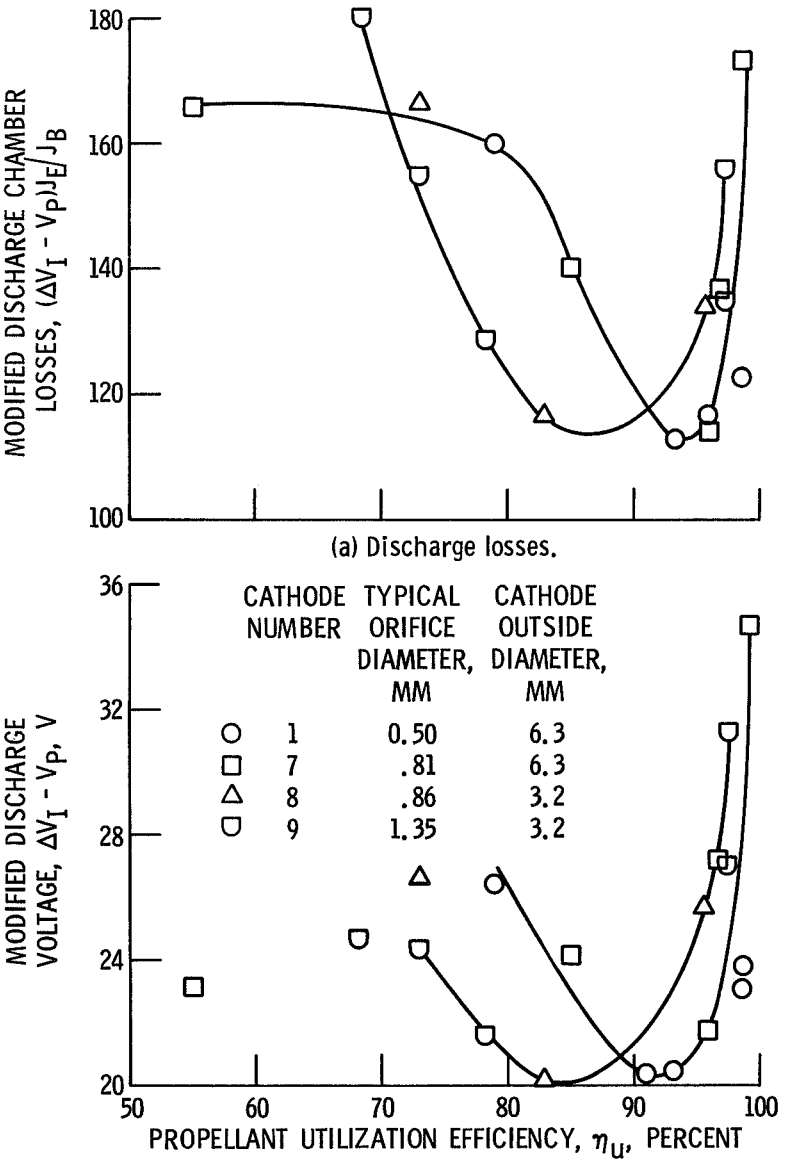

(a) Discharge losses.

(b) Discharge voltage.

Figure 13. - Thruster operating parameters for different cathodes with correction for distributor pole piece plasma potential. Emission current, 8 A.

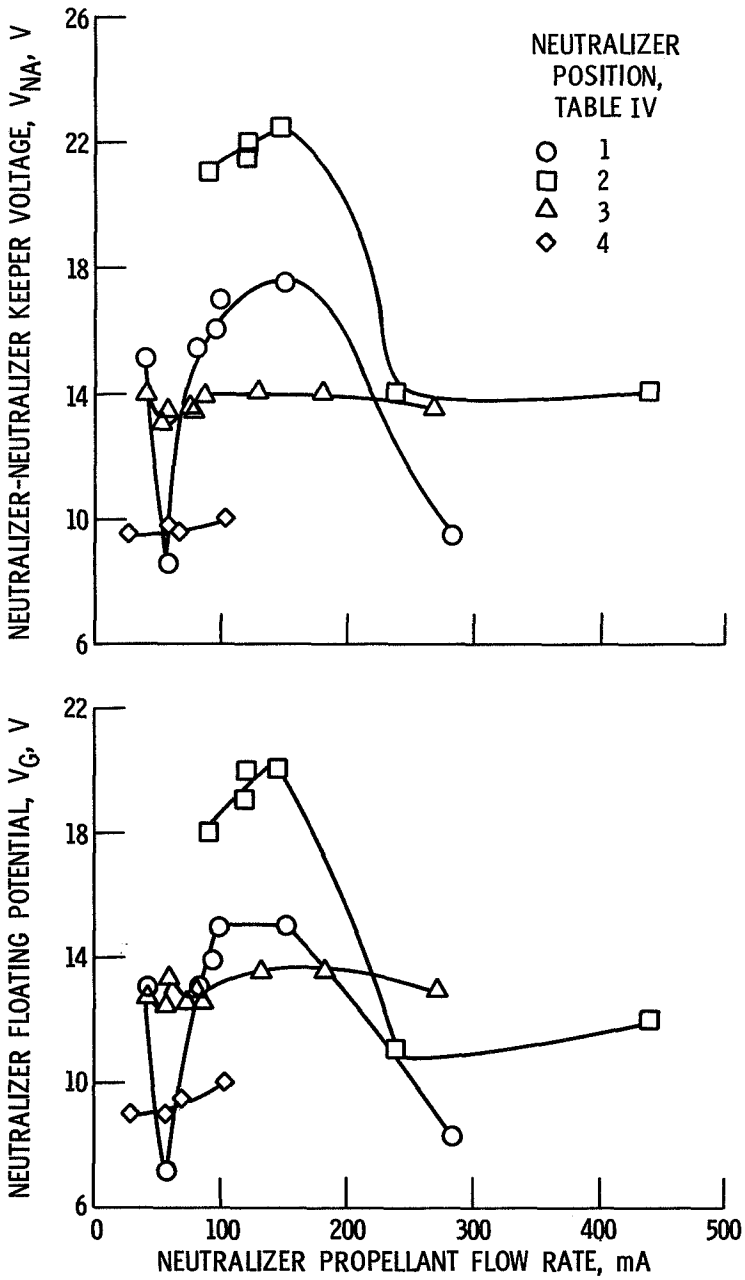

Figure 14. - Neutralizer operating voltages as a function of neutralizer propellant flow rate. Net accelerating potential, 1000 V; accelerator potential, -500 V; beam current, 1.5 A.

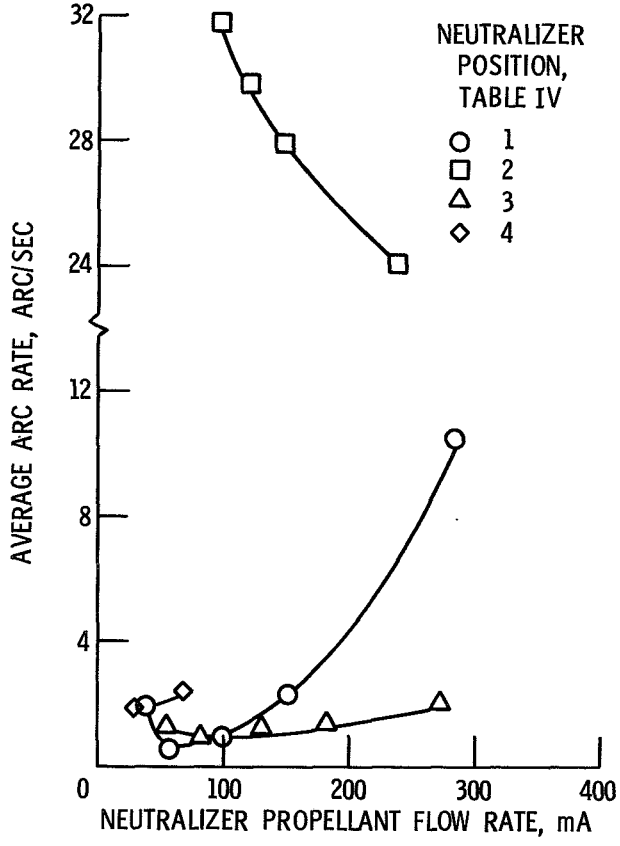

Figure 15. - Accelerator transient arc rate as a function of neutralizer propellant flow rate. Net accelerating potential, 1000 V; accelerator potential, -500 V; beam current, 1.5 A.

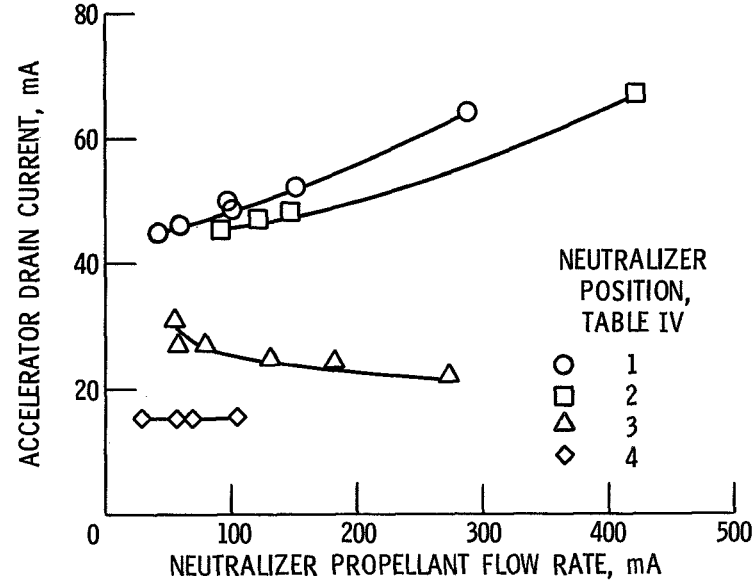

Figure 16. - Accelerator impingement current as a function of neutralizer propellant flow rate. Net accelerating potential, 1000 V; accelerator potential, -500 V; beam current, 1.5 A.